Supporting Information

Scaling analyses for hyperpolarization transfer across a spin-diffusion barrier and into bulk solid media

Nathan A. Prisco,[1] Arthur C. Pinon,[2] Lyndon Emsley,[2] and Bradley F. Chmelka[1]*

[1] Department of Chemical Engineering, University of California, Santa Barbara, California, USA 93106

[2] Institut des Sciences et Ingénieure Chimiques, École Polytechnique Fédérale de Lausanne, CH-1015 Lausanne, Switzerland

Table of contents

Section S1. Experimental data and calibration

Schematic pulse sequences and representative spectra used for the determination of characteristic times (T_1/T_{DNP}), the NMR signal enhancement (ε_∞), and the depolarization factor (θ_{depo}) are given in Figure S1. Characteristic times are measured by incrementing τ_1 delays and measuring the recovery of NMR signal intensity following a train of saturation pulses. The NMR signal enhancement (ε_∞) is the ratio of signal intensity between the microwave on and microwave off spectra. During the echo delay ($2\tau_2$ = 160 μs), broad ^{1}H signal intensity from the probe background and strongly hyperfine-coupled nuclei are significantly broadened and partially dephased due to their relatively short T_2 relaxation times. Consequently ^{1}H spin-echo experiments preferentially detect diamagnetic ^{1}H species in the frozen solvent matrix. It is assumed for all calculations that $T_{DNP} \equiv T_{DNP(on)} \approx T_{DNP(off)}$, since these values are generally within 10% of each other as reported in Table S1; noting that $T_{DNP(on)}$ values are used for all analyses presented in the main text. Only at 2 mM AMUPol concentrations and high glycerol-water ^{1}H spin densities, ρ_H > 50 M, are the $T_{DNP(off)}$ values appreciably longer. This may be attributed to microwave heating, a greater weighting of faster-relaxing hyperpolarized ^{1}H species near paramagnetic centers, or due to a slightly differences in the apparent rate constant, k_{DNP}, in the presence or absence of microwave irradiation. Regardless, these quantities are of the same order of magnitude suggesting that polarization transfer across the spin-diffusion barrier is similarly impeded both in the presence and absence of microwave irradiation.

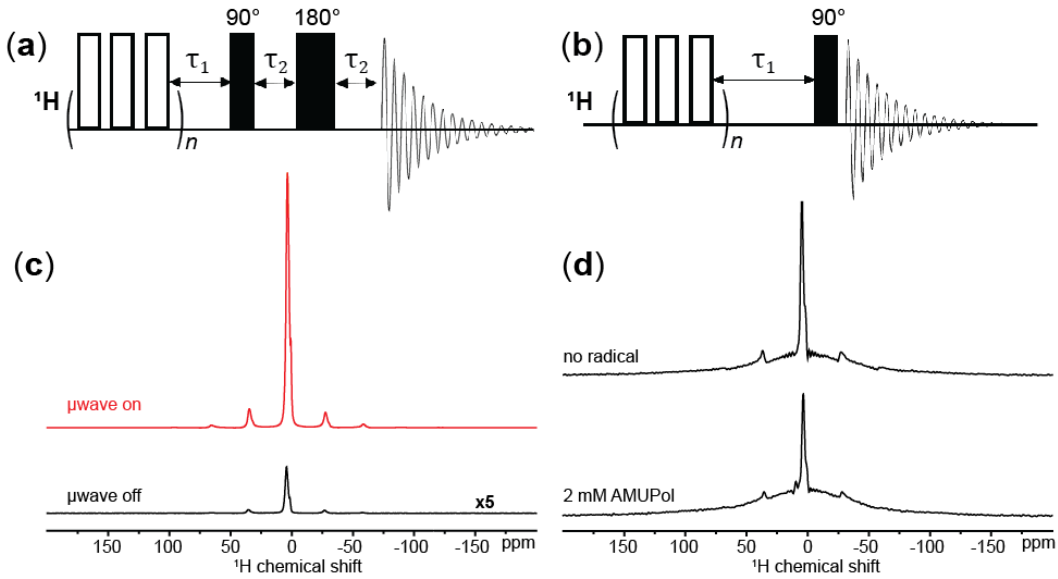

Figure S1. (a) Pulse sequence for spin-echo ^{1}H saturation recovery experiment with n = 20 saturation pulses, a fixed echo delay of $2\tau_2$ = 160 μs and a variable τ_1 delay. (b) Pulse sequence for quantitative ^{1}H single-pulse measurements with n = 16 and a variable τ_1 delay. (c) Spin-echo ^{1}H spectra comparing μwave-on versus μwave-off signal intensity for 2 mM AMUPol in glycerol-water (ρ_H = 3.5 M) at 9.4 T, 100 K, 12.5 kHz MAS. (d) Quantitative ^{1}H signal intensity with and without 2 mM AMUPol in glycerol-water (ρ_H = 3.5 M) at 9.4 T, 100 K, 12.5 kHz MAS.

Table S1. Experimental characteristic build-up times of frozen 2 mM and 12 mM AMUPol glycerol-water matrices, as functions of ^{1}H spin density with and without microwave irradiation.

2 mM AMUPol			12 mM AMUPol		
ρ_H [M]	$T_{DNP,on}$ [s]	$T_{DNP,off}$ [s]	ρ_H [M]	$T_{DNP,on}$ [s]	$T_{DNP,off}$ [s]
3.5	28.1	26.0	1.3	9.1	8.2
7.8	20.6	19.5	3.5	4.7	4.4
13	15.4	15.6	7.9	3.3	3.1
23	13.5	14.5	14	2.6	2.6
32	13.5	14.6	28	2.4	2.5
52	13.7	15.0	56	2.5	2.8
92	13.1	15.0	108	2.9	3.1

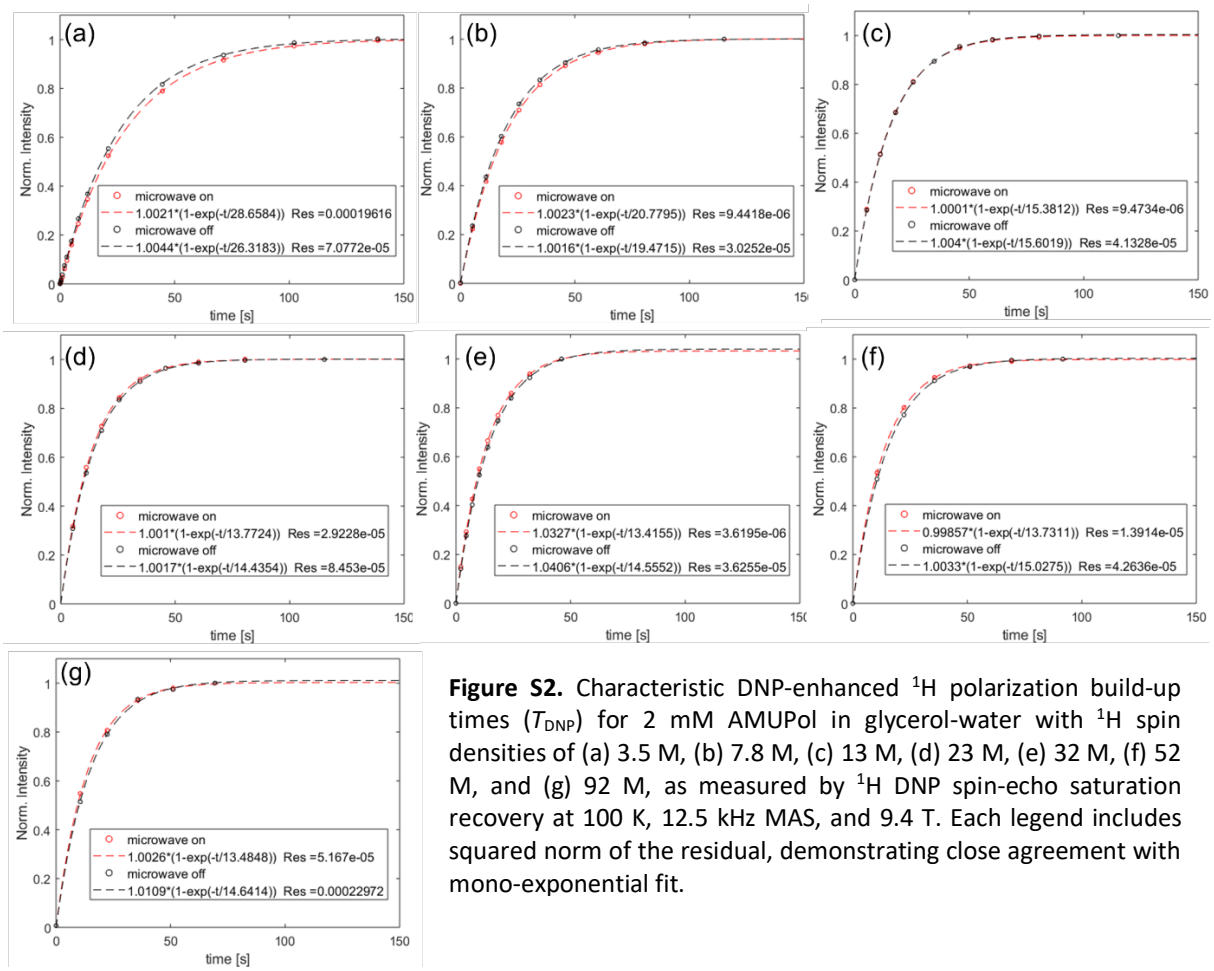

Figure S2. Characteristic DNP-enhanced ^{1}H polarization build-up times (T_{DNP}) for 2 mM AMUPol in glycerol-water with ^{1}H spin densities of (a) 3.5 M, (b) 7.8 M, (c) 13 M, (d) 23 M, (e) 32 M, (f) 52 M, and (g) 92 M, as measured by ^{1}H DNP spin-echo saturation recovery at 100 K, 12.5 kHz MAS, and 9.4 T. Each legend includes squared norm of the residual, demonstrating close agreement with mono-exponential fit.

In the presence of paramagnetic centers, ^{1}H signal intensity is partially "bleached" by paramagnetic quenching or MAS-induced depolarization, where the DNP contribution factor (θ_{DNP}) is represented by the total fraction of remaining signal intensity, $\theta_{DNP} = \theta_{depo}\theta_q$, as determined from the experimental depolarization factor (θ_{depo}) and quenching factor (θ_q). [1] For dilute biradical concentrations (*e.g.*, 2 mM AMUPol) it may be assumed that paramagnetic quenching is negligible, $\theta_q = 1$, as quenching arises due to strong paramagnetic interactions near paramagnetic centers.[2] In contrast, depolarization effects are relayed through the diamagnetic bulk by spin diffusion similarly to a DNP enhancement. In Figure S3, depolarization factors are measured as a function of ^{1}H spin density by single-pulse ^{1}H NMR experiments. Although a linear calibration curve would be expected, the experimental curves are non-linear, Figure S3a, possibly due to dephasing by strong dipole interactions, r.f. inefficiencies, or a non-linear amplifier response. In Figure S3b, the depolarization factor as a function of ρ_H is determined from main text Eq. 12 using the

data in Figure S3a. The observed ρ_H dependence of the depolarization factor is consistent with quantum chemical simulations which have shown that nuclear depolarization decreases as solvent T_1 values decrease.[3]

For polystyrene in AMUPol glycerol-water suspensions, overlapping ^{1}H intensity prohibits the use of ^{1}H spin-echo saturation recovery measurements to measure signal enhancements and build-up times. Instead, ^{13}C-detected 1D ^{13}C{^{1}H} CP-MAS saturation recovery experiments are used to measure enhancements $\varepsilon_{\infty,M}$ and $\varepsilon_{\infty,S}$ values, shown in Fig. 5b in the main text. Similar to the enhancement values, characteristic build-up times are influenced by spin thermodynamic exchange between the dissimilar reservoirs. In Table S2, experimental polarization build-up times for polystyrene, $T_{DNP,S}$, and the DNP matrix, $T_{DNP,M}$, are compared with the, typically, much longer $T^o_{DNP,M}$ values corresponding to the homogeneous DNP matrix. Thus, at lower matrix $\rho_{H,M}$, polarization build-up times within the

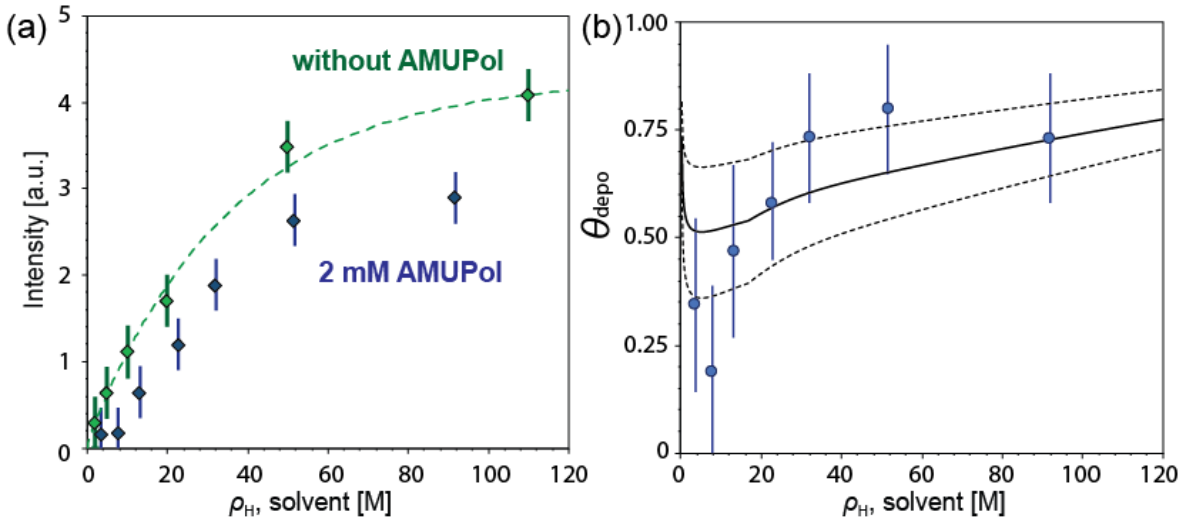

Figure S3. Quantitative single-pulse ^{1}H MAS NMR measurements of glycerol-water solutions at 9.4 T, 100 K, 12.5 kHz MAS, including (a) ^{1}H signal intensity with and without 2 mM AMUPol, and (b) DNP contribution factors ($\boldsymbol{\theta^o_{depo}}$), larger error bars include different masses of glycerol-water in the MAS rotor.

polystyrene particle interior are only weakly influenced by solvent-mediated ^{1}H spin diffusion. For such conditions, measured $T_{DNP,S}$ values are less than the ^{1}H spin-lattice relaxation time, $T^o_{1,S}$ = 1.3 s, indicating that particle surfaces are directly polarized by hyperfine transfer from adsorbed biradicals as discussed in the main text. Meanwhile at higher matrix $\rho_{H,M}$, measured $T_{DNP,S}$ values increase as the Zeeman spin conductivity of the matrix, $\rho_{H,M}\mathcal{D}_{H,M}C_z$, increases. In general, DNP matrices with higher Zeeman spin conductivities (larger $\rho_{H,M}$) can more effectively relay hyperpolarization to a solid-particle sink. However, because DNP generation rates are limited by the spin-diffusion barrier, higher $\rho_{H,M}\mathcal{D}_{H,M}C_z$ may lead to diminished polarization levels as discussed for the homogeneous DNP matrix in the main text.

Table S2: Experimental characteristic build-up times $T_{DNP,M}$ and $T_{DNP,S}$ for a suspension of polystyrene in 2 mM AMUPol glycerol-water with different ^{1}H densities.

$\rho_{H,M}$	1.3 M	4.0 M	12.5 M	25 M	108 M
$^{\dagger}T^o_{DNP,M}$ [s]	45.2	27.0	15.9	13.5	12.9
$T_{DNP,M}$ [s]	6.0	5.6	5.9	5.0	5.3
$T_{DNP,S}$ [s]	1.1	1.1	1.2	1.7	2.2

† values extracted from the solid-line in Fig. 3 in the main text

Section S2. Applying the lumped-element approximation

For Eqs. 4-6 in the main text it is assumed that a lumped-element approximation developed is valid. When spatial polarization gradients are negligible ($\nabla^2\tilde{P} = 0$), the bulk solvent matrix builds up uniformly to a single-polarization value for the hollow-sphere spanning from $\lambda_{sdb}<r<\lambda_{ws}$. Similar to lumped-parameter analyses in heat transfer processes, the following equation satisfies the First Law of Thermodynamics under a lumped-parameter assumption:

$$\rho_{\mathrm{H}} C_{\mathrm{z}} \frac{\partial \tilde{P}}{\partial t} = \dot{Q} + \rho_{\mathrm{H}} C_{\mathrm{z}} \frac{(1-\tilde{P})}{T_1} \tag{S1}$$

where the DNP source term per unit volume ($\dot{Q}$) is calculated by performing a surface integral of the polarization flux at the spin-diffusion barrier interface divided by the volume of bulk solvent:

$$\dot{Q} = \frac{1}{V} \cdot \iint (q_{\mathrm{H}} \cdot n) dS \quad , \tag{S2}$$

where n is the unit normal vector, and the surface integral is performed at $r = \lambda_{\mathrm{sdb}}$, which leads to:

$$\dot{Q} = \rho_{\mathrm{H}} C_{\mathrm{z}} k_{\mathrm{DNP}} L^{-1} \Delta \tilde{P} \quad . \tag{S3}$$

By substitution of Eq. S3 into Eq. S1, the following expressions are obtained describing polarization build-up with and without microwave irradiation:

$$\frac{\partial \tilde{P}}{\partial t} = \frac{\left(\frac{1 + k_{\mathrm{DNP}} L^{-1} \bar{P}_{\mathrm{CE(on)}} T_1}{1 + k_{\mathrm{DNP}} L^{-1} T_1} - \tilde{P}\right)}{T_1 / (1 + k_{\mathrm{DNP}} L^{-1} T_1)} \equiv \frac{(< \tilde{P}_{\mathrm{s.s.,on}} > - \tilde{P})}{T_{\mathrm{DNP,on}}} \tag{S4}$$

$$\frac{\partial \tilde{P}}{\partial t} = \frac{\left(\frac{1 + k_{\mathrm{DNP}} L^{-1} \bar{P}_{\mathrm{CE(off)}} T_1}{1 + k_{\mathrm{DNP}} L^{-1} T_1} - \tilde{P}\right)}{T_1 / (1 + k_{\mathrm{DNP}} L^{-1} T_1)} \equiv \frac{\left(< \tilde{P}_{\mathrm{s.s.,off}} > - \tilde{P}\right)}{T_{\mathrm{DNP,off}}} \quad , \tag{S5}$$

where $< \tilde{P}_{\mathrm{s.s.,on}} >$ and $< \tilde{P}_{\mathrm{s.s.,off}} >$ are the volume averaged steady-state polarization levels with and without microwave irradiation respectively in the bulk matrix ($\lambda_{\mathrm{sdb}} < r < \lambda_{\mathrm{ws}}$). As a consequence of the lumped-parameter approximation, the spatial dependence is removed, so that the polarization becomes a function of time only. These quantities, hereafter the absolute enhancement (ε_{θ}) and depolarization factor (θ_{depo}), are directly proportional to the net magnetization and, in principle, the NMR signal intensity.

Section S3. Error analysis for the lumped-element approximation

For high Biot number conditions, nuclear spin diffusion resistances in the bulk frozen glycerol-water matrix are expected to influence spatial polarization gradients, steady-state enhancements, and characteristic DNP build-up times. The lumped-parameter solution is no longer applicable as polarization-levels are diminished at distances progressively farther from the paramagnetic centers ($\nabla^2 \tilde{P} \neq 0$). The steady-state spatial polarization-level, $\tilde{P}_{\mathrm{s.s.}}(r)$, as a function of position, r, from the paramagnetic center may be solved for analytically. For an annular sphere spanning from $\lambda_{\mathrm{sdb}} < r < \lambda_{\mathrm{ws}}$, the steady-state general solution to Eq. 1 in the main text is given,

$$\tilde{P}_{\mathrm{s.s.}}(r) = 1 + \frac{C_I}{r} \cdot \cosh[\alpha^{-1} \cdot r] + \frac{C_{II}}{r} \cdot \sinh[\alpha^{-1} \cdot r] \tag{S6}$$

where $\alpha = \sqrt{\mathcal{D}_{\mathrm{H}} T_1}$ and the boundary conditions are:

Boundary Condition #1: $\tilde{P}_{\mathrm{s.s.}}|_{\lambda_{\mathrm{sdb}}}$ at $r = \lambda_{\mathrm{sdb}}$

Boundary Condition #2: $\frac{\partial \tilde{P}}{\partial r}|_{\lambda_{\mathrm{ws}}} = 0$

assuming a homogeneous distribution of paramagnetic centers with a mean separation distance represented by twice the Wigner-Seitz radius, $2\lambda_{\mathrm{ws}}$. Here α represents the characteristic diffusion length which is >100 nm for frozen glycerol-water solutions at 9.4 T, 100 K, and 12.5 kHz MAS. The integration constants C_{I} and C_{II} may be solved by application of the B.C.s to obtain:

$$C_I = \frac{\lambda_{\mathrm{sdb}} (\tilde{P}_{\mathrm{s.s.}}|_{\lambda_{\mathrm{sdb}}} - 1)}{\cosh(\alpha^{-1} \lambda_{\mathrm{sdb}}) - B_I \sinh(\alpha^{-1} \lambda_{\mathrm{sdb}})} \tag{S8}$$

$$C_{II} = -C_I B_I \tag{S9}$$

$$B_I = \frac{\lambda_{\mathrm{ws}}\alpha^{-1} \cdot \sinh(\lambda_{\mathrm{ws}}\alpha^{-1}) - \cosh\,(\lambda_{\mathrm{ws}}\alpha^{-1})}{\lambda_{\mathrm{ws}}\alpha^{-1} \cdot \cosh(\lambda_{\mathrm{ws}}\alpha^{-1}) - \sinh\,(\lambda_{\mathrm{ws}}\alpha^{-1})} \tag{S10}$$

where $\tilde{P}_{\mathrm{s.s.}}|_{\lambda_{\mathrm{sdb}}}$ is the steady-state nuclear polarization-level at the effective interface between hyperfine coupled ^{1}H nuclei and the bulk. This quantity may be determined by recognizing that for conservation of energy the energy flux flowing into the frozen solvent matrix at $r = \lambda_{\mathrm{sdb}}$, must equal the amount of energy being dissipated by spin-lattice relaxation over $\lambda_{\mathrm{sdb}} < r < \lambda_{\mathrm{ws}}$,

$$(q_H \cdot A)|_{\lambda_{\mathrm{sdb}}} = \iiint \rho_{\mathrm{H}} C_{\mathrm{z}} \frac{\left(\tilde{P}_{\mathrm{s.s.}}(r) - 1\right)}{T_1}\,\mathrm{dV} \tag{S11}$$

with respect to the Zeeman energy flux (q_H) and interfacial area (A) which yields,

$$\tilde{P}_{s.s.}|_{\lambda_{\mathrm{sdb}}} = \frac{\bar{P}_{CE} + \beta B_{II}/B_{III}}{1 + \beta B_{II}/B_{III}} \tag{S12}$$

$$B_{II} = -(\alpha^{-1}\lambda_{\mathrm{sdb}} + B_I)\sinh(\alpha^{-1}\lambda_{\mathrm{sdb}}) + (\alpha^{-1}\lambda_{\mathrm{sdb}}B_I + 1)\cosh(\alpha^{-1}\lambda_{\mathrm{sdb}}) + (\lambda_{\mathrm{ws}}\alpha^{-1} + B_I)\sinh(\lambda_{\mathrm{ws}}\alpha^{-1}) - (\lambda_{\mathrm{ws}}\alpha^{-1}B_I + 1)\cosh\,(\lambda_{\mathrm{ws}}\alpha^{-1}) \tag{S13}$$

$$B_{III} = \cosh(\alpha^{-1}\lambda_{\mathrm{sdb}}) - B_I \sinh(\alpha^{-1}\lambda_{\mathrm{sdb}}) \tag{S14}$$

where B_{I}, B_{II}, and B_{III} are geometry specific numerical constants. Importantly, β naturally arises as the dimensionless scaling parameter,

$$\beta = \frac{\alpha^2 {T_1}^{-1}}{k_{\mathrm{DNP}}\lambda_{\mathrm{sdb}}} \tag{S15}$$

that characterizes the ratio between the rate of energy dissipation in the bulk and the rate of energy transfer across a strong local magnetic field gradient (*e.g.*, the spin-diffusion barrier). This is analogous to the second Damköhler number ($\mathrm{Da_{II}}$), which is commonly used in interphase mass transfer to describe the dissolution of particles. Here, it compares the rate of polarization transfer to the bulk relative to the rate of polarization dissipation in the bulk. By comparing the low and high Biot number solutions, it is demonstrated that the condition of Bi<0.65 is sufficient to justify the use of a lumped-element approximation for 1D spherically symmetric geometry; the same condition used in heat transfer analyses. Future work will address fast-relaxing reservoirs which can also influence the validity of lumped-element approximations. The error in the lumped-element calculation is determined as follows:

$$\%\mathrm{error} = \frac{|\tilde{P}_{\infty,\mathrm{analytical}}(\lambda_{\mathrm{sdb}}) - \tilde{P}_{\infty,\mathrm{lumped}}(\lambda_{\mathrm{sdb}})|}{\tilde{P}_{\infty,\mathrm{analytical}}(\lambda_{\mathrm{sdb}})} \times 100\% \tag{S16}$$

where $\tilde{P}_{\infty,\mathrm{lumped}}(\lambda_{\mathrm{sdb}})$ is the solution developed in Section S2 above and $\tilde{P}_{\infty,\mathrm{analytical}}(\lambda_{\mathrm{sdb}})$ is the solution developed by Eqs. S6 – S15, the calculated error is presented in Figure S4 for a 2 mM AMUPol in glycerol-water matrix.

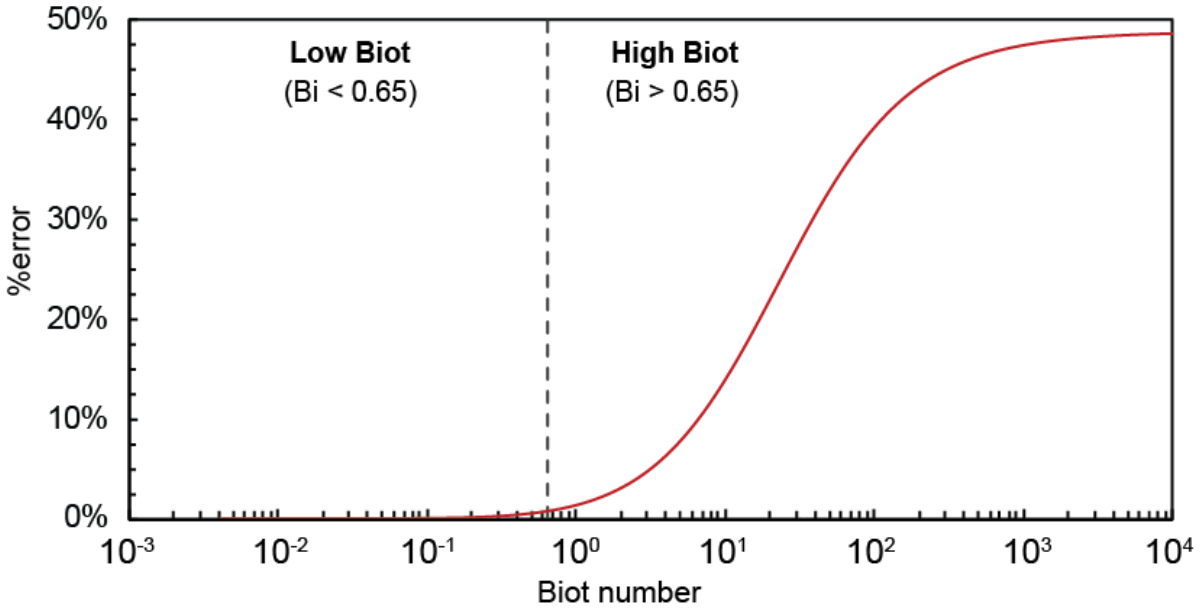

Figure S4. Calculated %error of the lumped-element approximation for a 2 mM AMUPol in glycerol-water matrix under the conditions described in the main text.

Section S4. Derivation of the effectiveness factor (η)

For hyperpolarization transfer to a solid particle sink of radius R facilitated solely by DNP matrix mediated spin-diffusion, from Eq. 7 in the main text, the internal dissipation of hyperpolarization over $0 < r < R$ is given,

$$\frac{\partial \tilde{P}_S}{\partial \tilde{t}} = \emptyset_S{}^{-2} \cdot \tilde{\nabla}^2 \tilde{P}_S - (\tilde{P}_S - 1) \tag{S17}$$

Boundary Condition #1: $\lim_{\tilde{r}\to 0} \frac{\partial \tilde{P}_S}{\partial \tilde{r}} = 0$

Boundary Condition #2: $\tilde{P}_S|_{\tilde{r}=1}\ at\ \tilde{r} = 1$

where the Thiele modulus of the solid-particle, $\emptyset_S = R/\sqrt{\mathcal{D}_{\mathrm{H},S} T^{\mathrm{o}}_{1,S}}$, is obtained using $\tilde{r} = r/R$ and $\tilde{t} = t/T^{\mathrm{o}}_{1,S}$ respectively. By application of the boundary conditions, the following steady-state solution is obtained for $\tilde{P}_S(r)$, the spatial polarization profile within the particle interior,

$$\tilde{P}_S(\tilde{r}) = 1 + \frac{(\tilde{P}_S|_{\tilde{r}=1} - 1)}{\tilde{r}} \cdot \frac{\sinh[\emptyset_S \cdot \tilde{r}]}{\sinh[\emptyset_S]} \tag{S18}$$

where the polarization at the particle surface, $\tilde{P}_S|_{\tilde{r}=1}$, is maintained by the rates of hyperpolarization generation and propagation in the DNP matrix. The effectiveness factor (η) is defined as the ratio between the energy dissipation rate throughout the solid-particle ($\bar{Q}_{\mathrm{actual}}$) and the theoretical maximum energy dissipation rate ($\bar{Q}_{\mathrm{max}}$) which would occur if the entire particle was polarized uniformly to the polarization-level at the particle surface,

$$\eta = \bar{Q}_{\mathrm{actual}} \Big/ \bar{Q}_{\mathrm{max}} \tag{S19}$$

with Zeeman energy dissipation rates of,

$$\bar{Q}_{\mathrm{max}} = \frac{4\pi R^3 \rho_{\mathrm{H},S} C_{\mathrm{z}}}{3 T^{\mathrm{o}}_{1,S}} \cdot (1 - \tilde{P}_S|_{\tilde{r}=1}) \tag{S20}$$

$$\bar{Q}_{\mathrm{actual}} = \frac{4\pi R^3 \rho_{\mathrm{H},S} C_{\mathrm{z}}}{3 T^{\mathrm{o}}_{1,S}} \cdot (1 - < \tilde{P}_S >) \tag{S21}$$

with $< \tilde{P}_{S,\infty} >$ corresponding to the average steady-state polarization of the solid-particle interior. This is obtained by integration of the steady-state solution as follows,

$$< \tilde{P}_S > = 3 \int_0^1 \tilde{P}_S(\tilde{r}) \cdot \tilde{r}^2 \, d\tilde{r} \tag{S22}$$

Evaluating this integral, and computing the effectiveness factor to obtain,

$$\eta = 3\emptyset_S{}^{-2} \cdot (\emptyset_S \cdot \coth[\emptyset_S] - 1) \tag{S23}$$

Importantly η provides a simple index to relate the polarization-level at the surface with the average polarization accrued through the particle interior. For DNP-NMR experiments, the absolute polarization enhancement, $\varepsilon_{\theta,S}$, and depolarization factor, $\theta_{\mathrm{depo},S}$, are related to the surface polarization by,

$$\varepsilon_{\theta,S} = \eta(\tilde{P}_{S(\mathrm{on})}|_{\tilde{r}=1} - 1) + 1 \tag{S24}$$

$$\theta_{\mathrm{depo},S} = \eta(\tilde{P}_{S(\mathrm{off})}|_{\tilde{r}=1} - 1) + 1 \tag{S25}$$

in the presence and absence of microwave irradiation respectively. To explicitly determine $\tilde{P}_{S(\mathrm{on})}|_{\tilde{r}=1}$ and $\tilde{P}_{S(\mathrm{off})}|_{\tilde{r}=1}$ additional information is needed regarding the efficacy of hyperpolarization transfer to the particle surface.

Section S5. Efficacy of hyperpolarization transfer to a particle surface

For hyperpolarization transfer to a spherical particle sink (*S*) of radius *R* coated with a DNP matrix (*M*) of thickness ΔR_{eff}, Eq. 7 in the main text corresponds to:

$$\rho_{\mathrm{H},M} C_{\mathrm{z}} \frac{\partial \tilde{P}_M}{\partial t} = \nabla\left(\rho_{\mathrm{H},M} C_{\mathrm{z}} \mathcal{D}_{\mathrm{H},M} \nabla \tilde{P}_M\right) - \rho_{\mathrm{H},M} C_{\mathrm{z}} \frac{(\tilde{P}_M - \Xi_M)}{T^o_{DNP,M}} \tag{S26}$$

$$\rho_{\mathrm{H},S} C_{\mathrm{z}} \frac{\partial \tilde{P}_S}{\partial t} = \nabla\left(\rho_{\mathrm{H},S} C_{\mathrm{z}} \mathcal{D}_{\mathrm{H},S} \nabla \tilde{P}_S\right) - \rho_{\mathrm{H},S} C_{\mathrm{z}} \frac{(\tilde{P}_S - 1)}{T^o_{1,S}} \tag{S27}$$

I.C.

$$\tilde{P}_M(r,0) = \tilde{P}_S(r,0) = 0$$

$$\Xi_M = \begin{bmatrix} \varepsilon^o_{\theta,M}\,; \text{microwave on} \\ \theta^o_{\mathrm{depo},M}; \text{microwave off} \end{bmatrix}$$

B.C. #1

$$\tilde{P}_M(R,t) = \tilde{P}_S(R,t)$$

B.C. #2

$$\rho_{\mathrm{H},M} \mathcal{D}_{\mathrm{H},M} \frac{\partial \tilde{P}_M}{\partial r}|_R = \rho_{\mathrm{H},S} \mathcal{D}_{\mathrm{H},S} \frac{\partial \tilde{P}_S}{\partial r}|_R$$

B.C. #3

$$\lim_{r\to 0} \frac{\partial \tilde{P}_S}{\partial r} = 0$$

B.C. #4

$$\lim_{r\to(R+\Delta R_{\mathrm{eff}})} \frac{\partial \tilde{P}_M}{\partial r} = 0$$

assuming that hyperpolarization is solely delivered to the particle surface by DNP matrix-mediated spin diffusion. By nondimensionalizing of Eq. S26 using $\tilde{r} = r/R$ and $\tilde{t} = t/T^o_{1,S}$, respectively,

$$\frac{T^{\mathrm{o}}_{\mathrm{DNP},M}}{T^{\mathrm{o}}_{1,S}} \cdot \frac{\partial \tilde{P}_M}{\partial \tilde{t}} = \emptyset^*_M{}^{-2} \tilde{\nabla}^2 \tilde{P}_M - (\tilde{P}_M - \Xi_M) \tag{S28}$$

where a composite Thiele modulus for the DNP matrix ($\emptyset^*_M$) in a heterogeneous solvent-solid suspension may be represented as,

$$\emptyset^*_M = \emptyset_S \sqrt{\frac{\mathcal{D}_{\mathrm{H},S} T^{\mathrm{o}}_{1,S}}{\mathcal{D}_{\mathrm{H},M} T^{\mathrm{o}}_{\mathrm{DNP},M}}} \tag{S29}$$

which yields the following steady-state solution,

$$\tilde{P}_{M,\infty}(\tilde{r}) = \Xi_M + \frac{C_{III}}{\tilde{r}} \cdot \cosh[\emptyset^*_M \cdot \tilde{r}] + \frac{C_{IV}}{\tilde{r}} \cdot \sinh[\emptyset^*_M \cdot \tilde{r}] \tag{S30}$$

where the integration constants C_{III} and C_{IV} are most conveniently obtained by application of B.C.s #1 and #4. However, as was the case for Eq. S18, this yields the steady-state spatial polarization profile within the DNP matrix $\tilde{P}_{M,\infty}(\tilde{r})$ in terms of, $\tilde{P}_S|_{\tilde{r}=1}$, the unknown surface polarization. For conservation of energy, the rate of energy

dissipation within the solid-particle interior must be equal to the rate of energy flowing into the particle surface at steady-state imposing the condition,

$$4\pi R^2 \rho_{\mathrm{H},M} C_{\mathrm{z}} \mathcal{D}_{\mathrm{H},M} \frac{\partial \tilde{P}_M}{\partial r} = \bar{Q}_{\mathrm{actual}} \tag{S31}$$

$$\bar{Q}_{\mathrm{actual}} \equiv \eta \bar{Q}_{\mathrm{max}} = -\frac{4\pi R^3 \rho_{\mathrm{H},S} C_{\mathrm{z}}}{3T_{1,S}^{\mathrm{o}}} \cdot \eta(1 - \tilde{P}_S|_{\tilde{r}=1}) \tag{S32}$$

where η is the solid-particle effectiveness factor. By nondimensionalization Eq. S31 is then,

$$\frac{\partial \tilde{P}_M}{\partial \tilde{r}}|_{\tilde{r}\,=\,1} = \tfrac{1}{3}\mathrm{Da}_{\mathrm{P}} \cdot \eta(\tilde{P}_S|_{\tilde{r}=1} - 1) \tag{S33}$$

where the polarization analogue of the Damköhler number ($\mathrm{Da_P}$) for the frozen DNP solvent matrix is given,

$$\mathrm{Da}_{\mathrm{P}} = \frac{R^2 {T_{1,S}^{\mathrm{o}}}^{-1}}{\mathcal{D}_{\mathrm{H},M}} \cdot \frac{\rho_{\mathrm{H},S}}{\rho_{\mathrm{H},M}} \tag{S34}$$

which is the ratio between the rate of energy dissipation at the surface versus the rate of energy transfer to the surface by DNP matrix mediated spin-diffusion weighted with respect to the specific Zeeman heat capacity of each medium. From which it may be demonstrated that,

$$\tilde{P}_M(\tilde{r}) = \Xi_M - \Gamma_I \frac{\frac{1}{3}\mathrm{Da}\,\eta\left(\tilde{P}_S|_{\tilde{r}=1} - 1\right)}{\sinh[\emptyset_M^*] - \Gamma_{II}\cosh[\emptyset_M^*]} \cdot \left(\frac{\sinh[\emptyset_M^* \cdot \tilde{r}]}{\tilde{r}} - \Gamma_{II}\frac{\cosh[\emptyset_M^* \cdot \tilde{r}]}{\tilde{r}}\right) \tag{S35}$$

$$\tilde{P}_S|_{\tilde{r}=1} = \frac{\Xi_M + \frac{\mathrm{Da_P}\eta}{3\Gamma_I}}{1 + \frac{\mathrm{Da_P}\eta}{3\Gamma_I}} \tag{S36}$$

where Γ_I and Γ_{II} are geometry specific numerical constants,

$$\Gamma_I = -\frac{\tanh[\emptyset_M^*] - \Gamma_{II}}{\emptyset_M^* + \Gamma_{II} - \tanh[\emptyset_M^*] \cdot (1 + \emptyset_M^*\Gamma_{II})} \tag{S37}$$

$$\Gamma_{II} = \frac{\zeta\emptyset_M^* - \tanh[\zeta\emptyset_M^*]}{\zeta\emptyset_M^* \cdot \tanh[\zeta\emptyset_M^*] - 1} \tag{S38}$$

where $\zeta = 1+\Delta R_{\mathrm{eff}}/R$ corresponds to the $\tilde{r}$ boundary position of the DNP solvent matrix. From Eq. S36, the steady-state solid enhancement, $\varepsilon_{\theta,S} \equiv < \tilde{P}_{S(\mathrm{on})} >$, or depolarization factor, $\theta_{\mathrm{depo},S} \equiv < \tilde{P}_{S(\mathrm{off})} >$, is calculated,

$$< \tilde{P}_S >= 3\int_0^1 \tilde{P}_S(\tilde{r}) \cdot \tilde{r}^2 d\tilde{r} \tag{S39}$$

$$< \tilde{P}_S >= \eta\left(\frac{\Xi_M + \frac{\mathrm{Da_P}\,\eta}{3\Gamma_I}}{1 + \frac{\mathrm{Da_P}\,\eta}{3\Gamma_I}} - 1\right) + 1 \tag{S40}$$

importantly the measured NMR signal enhancement, $\varepsilon_{\infty,S} \equiv < \tilde{P}_{S(\mathrm{on})} > / < \tilde{P}_{S(\mathrm{off})} >$, may be obtained directly from Eq. S40. This analytical solution is used to generate the dotted lines in Fig. 5b in the main text.

Section S6. Comparison of lumped-element solution with previous *ab initio* predictions

As discussed in the main text, by invoking a DNP transfer coefficient, k_{DNP}, the polarization build-up rates and gain may be quantitatively predicted from values of k_{DNP} and $\overline{P}_{CE}$ for materials with different compositions and bulk spin-lattice relaxation properties. In particular, previous quantum mechanical simulations[3] (Mentink-Vigier, et al., *Phys. Chem. Chem. Phys*., **2017** *19*, 3506, ref. [23] in the main text) have calculated the dependences of T_1 vs. T_{DNP} and T_1 vs. ε_θ^o, which may be directly compared to the predictions of Equations 5a, 6 and 7 in the main text. As shown in Figure S5 below, the crosses correspond to simulated values extracted from reference [3] corresponding to a simulation of a "TOTAPol-like" isolated biradical. Although the description of the system does not specify a biradical concentration, the extracted $k_{DNP}L^{-1}$ value of 0.137 s^{-1} is bounded between those measured in the present study. From the data in the main text, $k_{DNP}L^{-1}$ values range from 0.03 – 0.06 s^{-1} and 0.10 – 0.40 s^{-1} for 2 mM or 12 mM AMUPol glycerol-water matrices, respectively, with varying extents of deuteration. The simulation results predict polarization build-up rates that agree with values expected for commonly used DNP matrix formulations. Also from the simulation, by keeping $k_{DNP}L^{-1}$ constant, the effective polarization-level of core nuclei under microwave irradiation, $\bar{P}_{CE(on)}$, may be obtained, as shown in Figure S5b. Again, the simulated value is in agreement with the value of $\bar{P}_{CE(on)}$ = 148 ±14 measured for 2 mM AMUPol in a frozen glycerol-water matrix. Although the depolarization factor was not measured for 12 mM AMUPol solutions in this work, using the data provided in Fig. 2b of reference [4] and the enhancement factors reported in Table S3 below, a value of $\bar{P}_{CE(on)}$ = 75 ±5 is estimated for 12 mM AMUPol. Therefore it may be concluded that the $\bar{P}_{CE(on)}$ value associated with the simulated data is a realistic estimate bounded by the conditions used in the present study. The *ab initio* simulation results accurately describe cross-effect events, which might be expected to generate a ^{1}H nuclear spin polarization as high as 658. Within the context of the film-transfer model, this is not the maximum predicted enhancement that can be physically delivered to bulk ^{1}H nuclei. It appears that the simulation predicts a similar limit to the maximum ^{1}H polarization level that can be delivered to the bulk. Specifically, $\bar{P}_{CE(on)}$ = 104.5 corresponds to the asymptotic limit of the curve in Figure S5b, as the bulk T_1 value approaches infinity. From the present work, this value is clearly less than 658, the reason for which is not clear, but may be due to electron spin relaxation effects, as discussed in the main text.

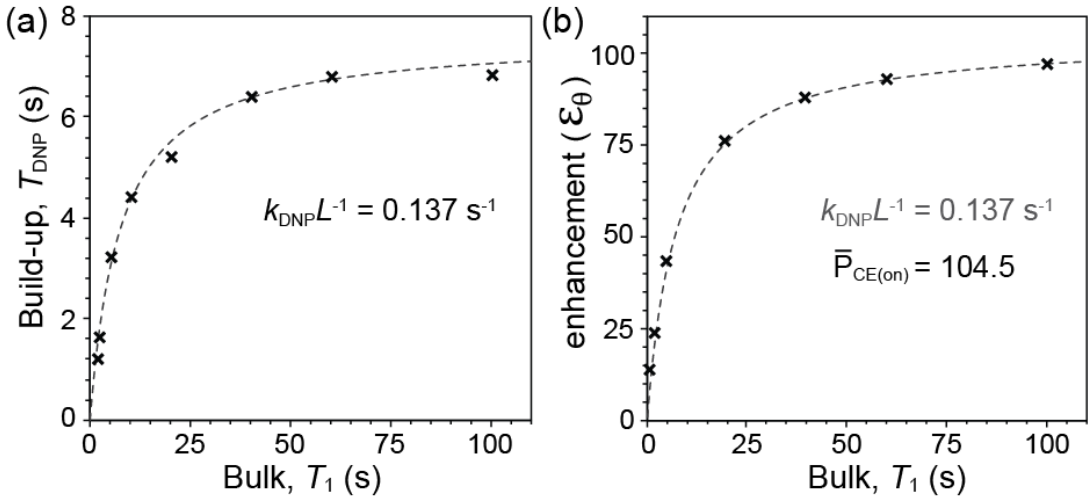

Figure S5. Comparison of results from the lumped-element solution presented here (Eqs. 5a, 6, and 7 in the main text) with those of *ab initio* calculations from Mentink-Vigier, et al., *Phys. Chem. Chem. Phys*., **2017** *19*, 3506 with data for (a) T_1 vs. T_{DNP} and (b) T_1 vs. ε_θ^o extracted from Figure 9 in reference [3].

Table S3: Experimental ε_∞ values and calculated $\bar{P}_{CE(on)}$ values of frozen 12 mM AMUPol glycerol-water matrices as functions of ^{1}H spin density

$\rho_{H,M}$	1.3 M	3.5 M	7.9 M	14 M	28 M	56 M	108 M
ε_∞	247	265	254	243	213	184	176
$^\dagger\bar{P}_{CE(on)}$	80	81	78	76	71	67	75

*Value of $\bar{P}_{CE(off)} = 0.28$ is calculated using θ^o_{depo}= 0.305 (10 kHz MAS) from Fig. 2b in reference [4] and from Eq. 7 in the main text with T_1^o = 79 s and $k_{DNP}L^{-1}$ = 0.38 s^{-1} corresponding to 12 mM AMUPol in glycerol-water (ρ_H = 14 M).
†Values of $\bar{P}_{CE(on)}$=75 ±5 calculated from Eq. 7 in the main text and averaged for values in Table S3.

Section S7. Calculation of DNP injection rates

For 2 mM AMUPol in glycerol-water the DNP injection rate in units of W/biradical may be straightforwardly calculated from the reported k_{DNP} and $\bar{P}_{\mathrm{CE}}$ values. At steady-state, the energy being dissipated by T_1 relaxation processes must exactly match that being delivered into the bulk across the spin-diffusion barrier. The rate of energy dissipation by T_1 relaxation processes is,

$$Q_{\mathrm{con}} = -\int_{\lambda_{\mathrm{sdb}}}^{\lambda_{\mathrm{ws}}} \rho_{\mathrm{H}} C_{\mathrm{z}} \cdot \frac{\tilde{P}(r) - 1}{T_1} 4\pi r^2 dr \tag{S41}$$

which for low Biot conditions is simply,

$$Q_{\mathrm{con}} = -\frac{4\pi}{3}(\lambda_{\mathrm{ws}}{}^3 - \lambda_{\mathrm{sdb}}{}^3)\rho_{\mathrm{H}} C_{\mathrm{z}} \cdot \frac{\varepsilon_\theta - 1}{T_1} \tag{S42}$$

under conditions of microwave irradiation. By comparison the rate of hyperpolarization transfer to bulk nuclei is represented by,

$$Q_{\mathrm{gen}} = 4\pi\lambda_{\mathrm{sdb}}{}^2 \cdot \rho_{\mathrm{H}} C_{\mathrm{z}} k_{\mathrm{DNP}} (\bar{P}_{\mathrm{CE(on)}} - \varepsilon_\theta) \tag{S43}$$

and these expressions may be evaluated using reported $\bar{P}_{\mathrm{CE(on)}}$, k_{DNP}, and T_1 values in the main text. Equation S42 and S43 are evaluated and compiled for 2 mM AMUPol in glycerol-water in Table S3 below. The measured hyperpolarization rates are only tabulated for ^{1}H nuclei in the bulk spanning $\lambda_{\mathrm{sdb}} < r < \lambda_{\mathrm{ws}}$. The present analyses do not allow for the accounting of energy dissipation occurring among core ^{1}H nuclei, spectator nuclei (e.g., ^{2}H, ^{13}C), or energy which is transferred to reservoirs other than that of the Zeeman Hamiltonian. The DNP injection rate (W) in plotted in Figure S5a,b normalized with respect to the number of biradical molecules and the number of bulk ^{1}H nuclei, respectively.

Table S4. Calculation of DNP injection and dissipation rates by Equations S42 and S43 for 2 mM AMUPol in frozen glycerol-water matrices at 100 K, 12.5 kHz MAS, and 9.4 T.

ρ_{H} [M]	T_1 [s]	k_{DNP} [nm/s]	ε_θ	Q_{con} [W/biradical	Q_{gen} [W/biradical]
3.5	180	0.59	125	$-4.93\cdot10^{-23}$	$+4.93\cdot10^{-23}$
7.8	123	0.80	123	$-1.59\cdot10^{-22}$	$+1.59\cdot10^{-22}$
13	83	1.05	121	$-3.86\cdot10^{-22}$	$+3.86\cdot10^{-22}$
23	53	1.09	111	$-9.60\cdot10^{-22}$	$+9.60\cdot10^{-22}$
32	42	1.00	101	$-1.50\cdot10^{-21}$	$+1.50\cdot10^{-21}$
52	34	0.86	89	$-2.74\cdot10^{-21}$	$+2.74\cdot10^{-21}$
92	25	0.71	70	$-5.25\cdot10^{-21}$	$+5.25\cdot10^{-21}$

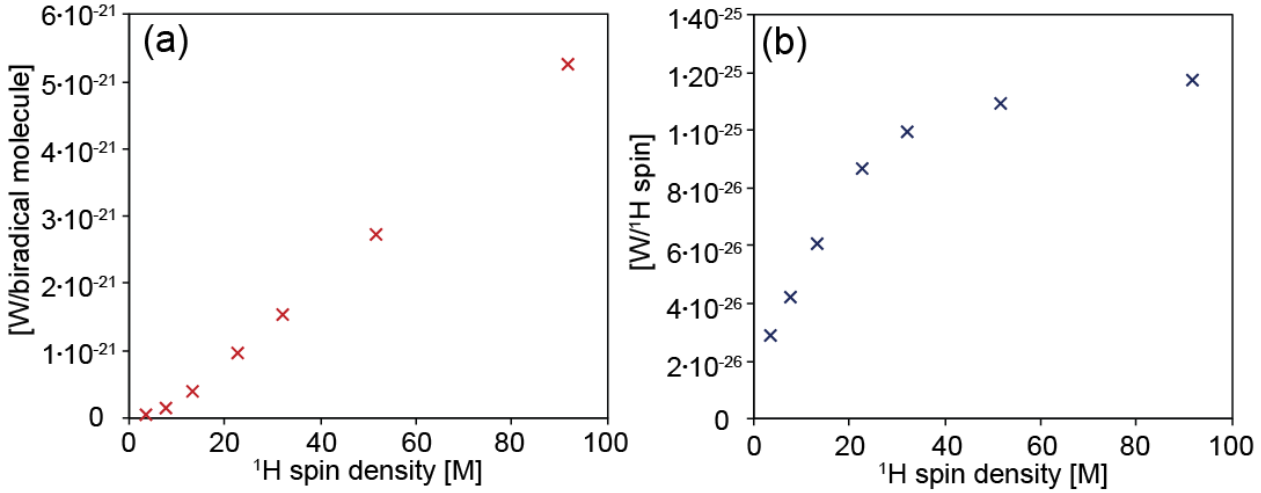

Figure S6. DNP injection rates (W) normalized with respect to (a) the number of biradical molecules, or (b) the number of bulk ^{1}H nuclei, respectively, as measured for 2 mM AMUPol in glycerol-water at 9.4 T, 100 K, and 12.5 kHz MAS by ^{1}H spin-echo DNP saturation recovery and calculated from data in Table S3.

Section S8. Comparing Thermal, Mass, and Zeeman energy (spin-polarization) transfer

Table S5. Comparing Thermal, Mass, and Zeeman energy (spin polarization) transfer

Heat Conduction	$\boldsymbol{q = -k\nabla T}$ q ≡ heat flux in units of W m^{-2} k ≡ thermal conductivity in units of W m^{-1} K^{-1} ∇T ≡ temperature gradient in units of K m^{-1}
Molecular Diffusion (no ionic charge)	$\boldsymbol{j = -\mathcal{D}\nabla C}$ j ≡ molecular flux in units of mol s^{-1} m^{-2} $\mathcal{D}$ ≡ molecular diffusion coefficient in units of m^2 s^{-1} ∇C ≡ concentration gradient in units of mol m^{-4}
Spin Polarization Diffusion (homogeneous magnetic field)	$\boldsymbol{q_n = -\rho_n C_z \mathcal{D}_n \nabla P}$ q_n ≡ Zeeman energy flux in units of W m^{-2} $\mathcal{D}_n$ ≡ spin diffusion coefficient in units of m^2 s^{-1} ∇P ≡ spin polarization gradient in units of P' m^{-1} ρ_n ≡ nuclear spin density in units of mol m^{-3} C_z ≡ Zeeman heat capacity in units of W mol P'^{-1}

P' ≡ unitless polarization-level